The effect of strain on hot-electron and hole longitudinal diffusion and noise in Si and $Si_{0.9}Ge_{0.1}$

K. Yeom, J. M. Hinckley, and J. Singh
Department of Electrical Engineering and Computer Science, The University of Michigan, Ann Arbor, Michigan 48109-2122

(Received 12 May 1995; accepted for publication 29 June 1995)

Monte Carlo methods are used to model the electron and hole high-field transport in both unstrained and compressively strained silicon and silicon-germanium alloy. The data are analyzed to determine in what way the thermal noise properties of the carriers are affected by compressive, in-plane strain. Results include the longitudinal diffusion coefficient, the longitudinal noise temperature, and the longitudinal noise spectral density, for electric fields in the range of 0–20 kV/cm. The results are qualitatively similar for silicon with 1% compressive biaxial strain and for $Si_{0.9}Ge_{0.1}$/Si(001). The effects of strain are found to be more pronounced for electrons than for holes and are primarily related to changes in the conductivity effective mass. © *1995 American Institute of Physics.*

I. INTRODUCTION

Over the last decade, much interest has been focused on the electrical properties of the SiGe alloy, from the standpoint of forming heterostructure devices in a silicon-based technology. Both pseudomorphically strained and unstrained SiGe have been studied. Transport research in this area generally has been confined to the determination of the electron and hole mobilities, and their effect on device performance.[1,2] Detailed theoretical investigations of the second-order transport properties, diffusion, and thermal noise have not yet been fully pursued.

The diffusion coefficient of charge carriers in semiconductors generally is a function of electric field and for hot carriers may be significantly different from the low-field ohmic value. Knowledge of the diffusion coefficient at high fields is important for calculating both the operation and the noise properties of devices such as impact ionization avalanche transit time (IMPATT) diodes, field-effect transistors, and photodetectors.[3,4]

Much work has been reported for both theoretical and experimental determinations of the diffusion and noise properties of electrons and holes in silicon.[3–9] The purpose of the present work is to use Monte Carlo calculations to study how the charge-carrier longitudinal diffusion and noise properties in SiGe will be affected by compressive strain such as occurs in pseudomorphic layers. To do this, we proceed in three steps. First, we discuss the effects of compressive strain in Si. Here, the strain which we use is -1% in the $x-y$ plane and corresponds to that which would occur if the pure Si were grown as a layer on a (001) substrate with a 1% smaller lattice constant. This study is done to make clear what effects arise from strain, without the complicating issues associated with alloying. Second, we discuss the effects of alloying alone, without strain, in bulk $Si_{0.9}Ge_{0.1}$. This is done to show what effects arise from alloying, without including the effects of strain. Third, we discuss the simultaneous effects of alloying and strain in $Si_{0.9}Ge_{0.1}$/Si(001). In all cases we have restricted the discussion to the longitudinal characteristics, associated with motion and velocity fluctuations parallel to the applied electric field.

The rest of this article is organized into three further sections, as follows. Section II describes the modeling methods used, both the Monte Carlo methods and the formulas relating the diffusion and noise properties to the Monte Carlo output. Section III gives the results of the investigation for the three material systems: compressively strained Si, bulk SiGe, and $Si_{0.9}Ge_{0.1}$/Si(001). The results are stated in terms of the field dependence of the longitudinal diffusion coefficient D_l and the longitudinal noise temperature T_{nl}. In the case of strained SiGe we also give results for the longitudinal noise power spectral density S_l as a function of frequency. Section IV presents our conclusions.

II. MODELING

A. Monte Carlo

The models for the conduction band structure and electron scattering rates as well as the ensemble electron Monte Carlo implementation used in this work are generally described in Ref. 8. The band structure consists of six ellipsoidal valleys, with nonparabolicity. The constant energy surface is shown in Fig. 1(a). For the alloy, the longitudinal and transverse effective masses are linear interpolations of the respective masses in the X valleys for Si and Ge. Conduction-band deformation potential theory is used to model the effects of strain on the conduction-band structure.[10]

Biaxial strain, associated with a lattice-mismatched (001) substrate, shifts the energy of the two valleys which are perpendicular to the layer, with respect to the energy of the other four valleys, which are in the plane of the layer. The former two valleys move above the latter four valleys under compressive in-plane strain.[10] At energies below this strain-induced valley splitting, the conduction-band edge will be composed of only the four in-plane valleys. Figure 1(b) shows the near-band-edge electron constant energy surface that is characteristic of this situation. Only the four in-plane valleys are shown. The remaining two energy ellipsoids reappear only at higher energies, above the valley energy separation.

 0021-8979/95/78(9)/5454/6/$6.00

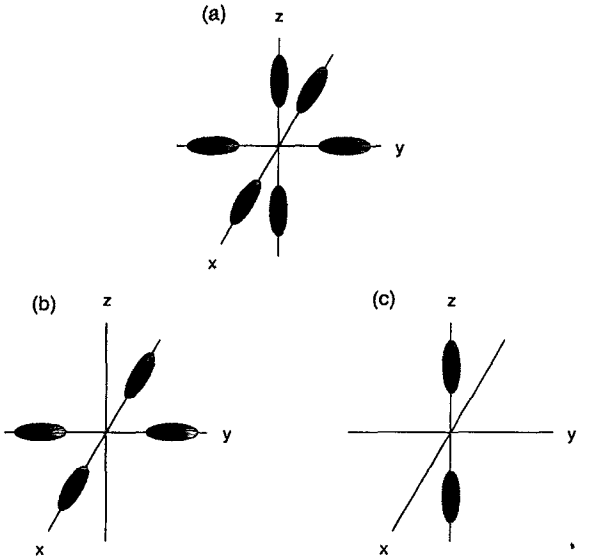

FIG. 1. Effect of strain on conduction-band edge. Schematic near-band-edge conduction-band constant energy surfaces in (a) unstrained silicon, (b) in-plane compressively strained ($\epsilon_{xx}=\epsilon_{yy}<0$) silicon, and (c) in-plane tensilely strained ($\epsilon_{xx}=\epsilon_{yy}>0$) silicon. In case (b), strain causes the two valleys on the z axis to be raised in energy, relative to the remaining four valleys, away from the band edge. In case (c), strain causes the four valleys on the x and y axes to be raised in energy, leaving the two valleys on the z axis to constitute the conduction-band edge.

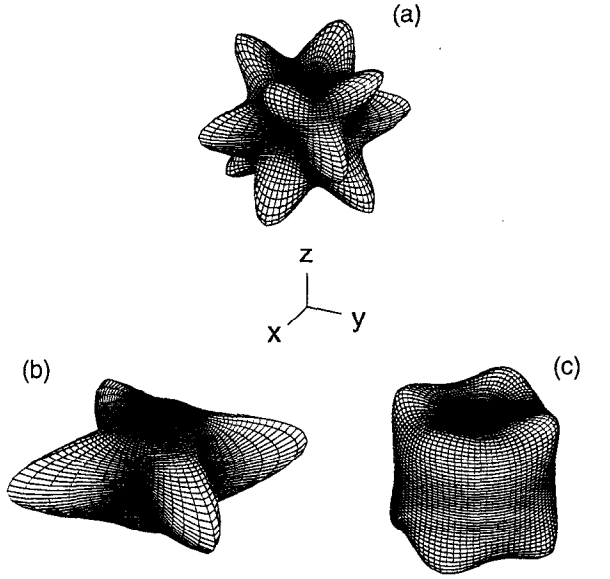

FIG. 2. Effect of strain on valence-band symmetry. Heavy-hole constant energy surfaces at 40 meV in (a) unstrained silicon, (b) in-plane compressively strained ($\epsilon_{xx}=\epsilon_{yy}<0$) silicon, and (c) in-plane tensilely strained ($\epsilon_{xx}=\epsilon_{yy}>0$) silicon. In the unstrained material (a), the highest effective mass occurs in the 12 symmetrically equivalent ⟨110⟩ directions. In the compressively strained material (b), the four ⟨110⟩ directions lying in the $x-y$ plane have greater effective mass than the eight equivalent ⟨101⟩ directions lying out of the $x-y$ plane. In the tensilely strained material (c), the situation is reversed, with the eight out-of-plane ⟨101⟩ directions exhibiting the highest effective mass.

The alternate situation of tensile in-plane strain has the converse effect on the electron band structure, pushing the four in-plane valleys higher in energy, above the two out-of-plane valleys. Figure 1(c) shows the near-band-edge electron constant energy surface that is characteristic of this situation. Only the two out-of-plane valleys are shown. As before, the remaining energy ellipsoids reappear only above the energy of the strain-induced valley separation.

In addition to the scattering processes of acoustic, optical, f-, and g-intervalley phonon scattering, as described in Ref. 8, random alloy[11] scattering is included in the simulations for both bulk $Si_{0.9}Ge_{0.1}$ and $Si_{0.9}Ge_{0.1}$/Si(001). An alloy scattering potential of $U_0=0.7$ eV was used.

The models of the valence-band structure and hole scattering rates as well as the hole Monte Carlo implementation used in this work have been described in substantial detail in separate publications.[10,12–14] This is a three-band ensemble Monte Carlo which models acoustic and nonpolar optical-phonon scattering of the holes. In the alloy, random alloy scattering, with an alloy scattering potential of $U_0=0.6$ eV,[15] is included.

Full anisotropy of the valence-band structure is obtained using a three-band $\mathbf{k}\cdot\mathbf{p}$ method including spin-orbit splitting. Strain is included via the valence-band deformation potential theory. Biaxial strain from epitaxial growth on a (001) substrate reduces the symmetry of the semiconductor from cubic to tetragonal. Figure 2 shows the effect of strain on the heavy-hole 40 meV constant energy surface. In Fig. 2(a), the constant energy surface for unstrained silicon is shown. The maxima occur along the 12 ⟨110⟩ directions. In Fig. 2(b) the constant energy surface for in-plane 1% compressively strained silicon is shown. Here the maxima occur along the four equivalent ⟨110⟩ directions, in the $x-y$ plane of the film. In Fig. 2(c) the constant energy surface for in-plane 1% tensilely strained silicon is shown. Here, the maxima occur along the eight equivalent ⟨101⟩ directions, out of the $x-y$ plane. The valence-band Monte Carlo includes the effects of strain in the band structure and the scattering rates, as described in Ref. 13.

B. Noise properties

Calculation of the noise properties from the Monte Carlo simulations, in this work, generally follows the discussion of Ref. 8. With the electric field oriented in the x direction, the longitudinal diffusion coefficient is calculated as

$$D_l=\frac{1}{2}\frac{d}{dt}\langle(\Delta x)^2\rangle, \tag{1}$$

where $\Delta x=x-\bar{x}$ is the position fluctuation. The angular brackets denote averaging over the carrier population. This form of the diffusion coefficient is known as the spreading diffusion coefficient. Another form is the noise diffusion coefficient, given by

$$D_l=\int_0^\infty\langle\Delta v_x(t)\Delta v_x(t+\tau)\rangle d\tau, \tag{2}$$

where $\Delta v_x=v_x-\overline{v_x}$, is the velocity fluctuation. These two forms of the diffusion coefficient are identical for static or steady state conditions.[3,4] In fact, they are the same for frequencies up to the reciprocal of the largest relaxation time

involved in the transport (e.g., ~100 GHz). The integrand of Eq. (2) is the velocity fluctuation autocorrelation function (in the x direction) $C_{xx}(\tau)$,

$$C_{xx}(\tau)=\langle \Delta v_x(t)\Delta v_x(t+\tau)\rangle. \tag{3}$$

Averaging over the carrier population makes this quantity independent of t.

More generally, diffusion can be obtained as a function of frequency,

$$D_l(\omega)=\int_0^\infty C_{xx}(\tau)\cos\,\omega\tau\, d\tau. \tag{4}$$

This is proportional to the longitudinal noise power spectral density $S_l(\omega)$.[6,7] The constant of proportionality is $4q^2nA/L$, where q is the electronic charge, n is the carrier density, A is the sample cross-sectional area, and L is the sample length.

The longitudinal noise temperature is given by an equation that formally looks like the Einstein relation,

$$T_{\rm nl}(E)=\frac{q}{k_B}\frac{D_l(E)}{\mu_d(E)}. \tag{5}$$

However, for $E\neq 0$, the system is not in thermodynamic equilibrium and Nyquist's relation is invalid. The quantities $D_l(E)$ and $\mu_d(E)$ are nonequilibrium values and generally $T_{\rm nl}$ is greater than the lattice temperature. In order to relate $T_{\rm nl}$ to noise power measurements, the differential mobility μ_d must be used in Eq. (5), not the chordal mobility.[3]

It should be noted that the formulas, presented above, are valid only under conditions in which carrier–carrier correlations may be neglected. Such correlations arise through carrier–carrier scattering. The scope of the present work is confined to intrinsic materials at $T=300$ K. At this temperature the intrinsic carrier concentration of silicon is 1.45×10^{10} cm^{-3}.[16] This is well below the typical room-temperature carrier concentrations of 10^{17} cm^{-3} where carrier–carrier scattering becomes important.[17] On this basis, the omission of carrier–carrier correlations is justified for silicon and the siliconlike alloy $Si_{0.9}Ge_{0.1}$ studied in this work.

Monte Carlo calculations are made of $\langle x^2\rangle$, $\langle x\rangle$ (or equivalently C_{xx}), and of the drift velocity, as functions of the electric field. Then $D_l(E)$ is obtained by Eq. (1) or (2). For zero field, the Einstein relation is used with the value of $D(0)$ to obtain the ohmic mobility. The slope of the velocity-field characteristic is taken to obtain the differential mobility for $E>0$. This is used in Eq. (5) to obtain the longitudinal noise temperature. The longitudinal noise power spectral density is obtained from the ratio of $D_l(\omega)$ [Eq. (4)] to $D_l(\omega=0)$. Taking the ratio avoids the need to specify the sample dimensions,

$$\frac{S_l(\omega)}{S_l(\omega=0)}=\frac{D_l(\omega)}{D_l(\omega=0)}=\frac{\int_0^\infty C_{xx}(\tau)\cos\,\omega\tau\, d\tau}{\int_0^\infty C_{xx}(\tau)d\tau}. \tag{6}$$

III. RESULTS

A. Effect of strain

The effects of strain on the electron and hole transport properties are shown in Fig. 3. The type of strain employed here, corresponding to biaxial lattice misfit on a (001) substrate with $\epsilon_{xx}=\epsilon_{yy}=-\sigma\epsilon_{zz}$, causes a distortion in which the lattice symmetry is changed from cubic to tetragonal. Therefore, while in the cubic, unstrained material $\langle 100\rangle$ corresponds to six equivalent directions, in the tetragonal, strained material [100] is not symmetrically equivalent to [001]. Thus, it is to be expected that the transport properties for electric fields oriented in the [100] direction will differ from those for electric fields oriented in the [001] direction. This has been born out in the results, with the difference being greater for electrons than for holes.

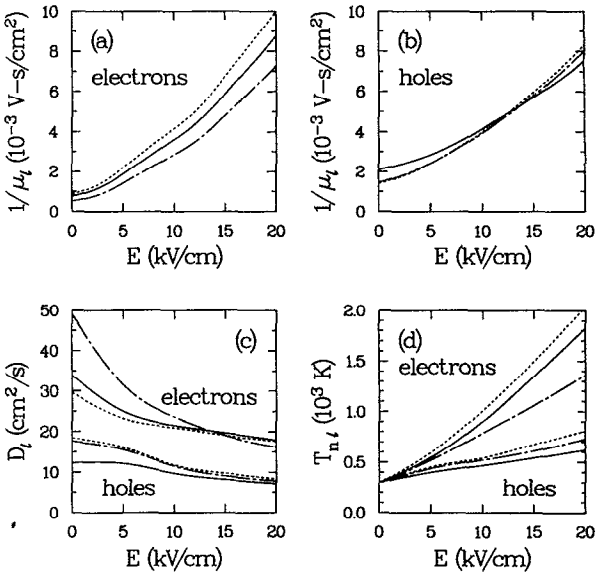

FIG. 3. Reciprocal differential mobility of (a) electrons and (b) holes, (c) longitudinal diffusion coefficient, and (d) longitudinal noise temperature for electrons and holes in unstrained and strained Si ($\epsilon_{xx}=\epsilon_{yy}=-0.010$, $\epsilon_{zz}=+0.0077$). In each figure, the solid lines pertain to unstrained silicon; the dotted lines pertain to strained silicon with $E\|[100]$; the dotted-dashed lines pertain to strained silicon with $E\|[001]$. In (c) and (d) the upper three curves are electron data and the lower three curves are hole data.

The effects of strain on the reciprocal of the differential mobility μ_d and on the longitudinal diffusion coefficient D_l are shown in Figs. 3(a)–3(c). The reciprocal mobility is shown to clarify the behavior of the noise temperature, which is proportional to the reciprocal of the mobility [Eq. (5)]. Compared to the case of bulk silicon, the mobility and diffusion coefficient of electrons in strained silicon increase for electric fields in the [001] direction, where the conductivity effective mass is m_t^*, and decrease for electric fields in the [100] direction, where the average conductivity effective mass is $2m_t^*m_l^*/(m_l^*+m_t^*)>m_t^*$. For holes, compared to the case of bulk silicon, the mobility and diffusion coefficient in strained silicon increase for electric fields in both the [001] and the [100] directions, because the conductivity effective mass decreases in both directions (slightly more in the [100] direction), under strain. The effect of strain on the longitudinal noise temperature, $T_{\rm nl}=qD_l/k_B\mu_d$, is shown in Fig. 3(d).

The data of Fig. 3 indicate that, as a result of strain, the longitudinal diffusivity D_l is reduced by a compressive in-plane strain. However, for low fields in the [001] direction,

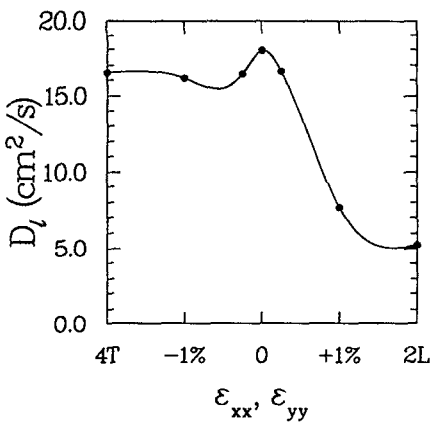

FIG. 4. Electron longitudinal diffusion coefficient as a function of in-plane biaxial strain ($\epsilon_{xx}=\epsilon_{yy}$), at an electric field of 20 kV/cm, perpendicular to the plane of the film, $E\|[001]$. The label "4T" refers to a very high negative strain, where all electrons are in the four in-plane valleys. The label "2L" refers to a very high positive strain, where all electrons are in the two out-of-plane valleys. Bulk, unstrained silicon data are at the center ($\epsilon_{xx}=\epsilon_{yy}=0$). Calculated data are denoted by closed circles; the solid line is only to aid viewing.

D_l is increased by a compressive in-plane strain. For $E\|[001]$, in the vicinity of 15 kV/cm, D_l (dotted-dashed line in the figure) becomes less than that for both bulk silicon and for the strained silicon with the field parallel to [100].

This surprising feature is clarified by considering the variation of the diffusion coefficient with respect to strain, for a constant electric field of 20 kV/cm. In Fig. 4, the diffusion coefficient is shown as a function of strain, ranging from the extreme case of very large negative strain, with conduction involving only the four in-plane valleys, which are perpendicular to the electric field, to the extreme case of very large positive strain, with the conduction involving only the two out-of-plane valleys, which are parallel to the electric field. The diffusion coefficient is seen to have a large value for negative strain, increase slightly to a maximum at zero strain, and to decrease abruptly for positive strain.

In general, the total diffusivity is a combination of intravalley diffusivity and intervalley diffusivity. The intravalley diffusivity pertains to the spreading of the carriers due to velocity fluctuations, while they stay within the group of the four in-plane valleys or within the group of the two out-of-plane valleys. The intervalley diffusivity pertains to the spreading of the carriers due to their scattering between the two valley groups, which have different characteristic drift velocities.

The total electron diffusivity D may be represented as the sum of three terms: the intravalley diffusivities in each of the two types of valley and an intervalley diffusivity term,[18]

$$D=\frac{\tau_4}{\tau_4+\tau_2}D_4+\frac{\tau_2}{\tau_4+\tau_2}D_2+n_2n_4(v_4-v_2)^2\tau_i, \qquad (7)$$

where D_4 and v_4 are the intravalley diffusivity and drift velocity characteristic of the four in-plane valleys, D_2 and v_2 are the corresponding quantities characteristic of the two out-of-plane valleys, and τ_i is the inverse intervalley scattering rate between the two types of valley. The time τ_4 is the inverse scattering rate from one of the four in-plane valleys to any of the two out-of-plane valleys. Conversely, the time τ_2 is the inverse scattering rate from one of the two out-of-plane valleys to any of the four in-plane valleys. The numbers n_2 and n_4 are the fractions of the carriers in the two out-of-plane valleys and in the four in-plane valleys, respectively. To a reasonable approximation in unstrained silicon, at the moderate fields that we are considering here,

$$\frac{\tau_4}{\tau_4+\tau_2}=n_4=2/3, \quad \frac{\tau_2}{\tau_4+\tau_2}=n_2=1/3. \qquad (8)$$

Using these values, the diffusivity for unstrained silicon is

$$D=\tfrac{2}{3}D_4+\tfrac{1}{3}D_2+\tfrac{2}{9}(v_4-v_2)^2\tau_i=\tfrac{2}{3}D_4+\tfrac{1}{3}D_2+D_i, \qquad (9)$$

where D_i is the intervalley diffusivity.

The values of D_4 and D_2 at $E=20$ kV/cm can be found in Fig. 4. In the case of extremely large in-plane compressive strain, all carriers occupy the four in-plane valleys ($n_4=1$, $n_2=0$) and $D=D_4$. This is the diffusivity shown for the strain limit labeled "4T" in Fig. 4. In the case of extremely large in-plane tensile strain, all carriers occupy the two out-of-plane valleys ($n_4=0$, $n_2=1$) and $D=D_2$. This is the diffusivity shown for the strain limit labeled "2L." Thus, from Fig. 4, $D_4=16.5$ cm^2/s and $D_2=5.1$ cm^2/s. As shown in the figure, $D=18.0$ cm^2/s, leading through Eq. (9) to a value for intervalley diffusivity for unstrained silicon of $D_i=5.3$ cm^2/s (at $E=20$ kV/cm).

Now, the reason for the crossing of the electron diffusivities in Fig. 3(c) should be evident. In the -1% strained silicon, virtually all of the carriers are in the four in-plane valleys. These valleys constitute the conduction-band edge and are substantially separated from the two higher out-of-plane valleys. The strained silicon electron diffusivity, with $E\|[001]$ in Fig. 3(c) (dotted-dashed line), is almost entirely the intravalley diffusivity for the four in-plane valleys, having the value of 16.1 cm^2/s at $E=20$ kV/cm. In the absence of intervalley diffusion, the data for unstrained silicon in Fig. 3(c) (solid line) would lie below this, having a value of $D=(2D_4+D_2)/3=12.7$ cm^2/s at $E=20$ kV/cm. However, the additional component of intervalley diffusivity raises the total diffusivity of unstrained silicon above that for strained silicon, where the field is perpendicular to the axes of the four in-plane energy ellipsoids.

The longitudinal noise temperature, shown in Fig. 3(d), exhibits no unexpected features, and follows the behavior of the reciprocal of the differential mobility. This is particularly evident in the high-field limit (20 kV/cm) where the reciprocal mobilities of electrons and holes are well separated for the different cases of strain, while the diffusivities have similar values between the different strain cases. Therefore, the longitudinal noise temperature is controlled by the mobility, which in turn is strongly affected by the changes in the conductivity effective masses, resulting from the strain.

B. Effect of alloying

The effects of alloying on the electron and hole transport properties are shown in Fig. 5. Unlike the effect under strain, the lattice retains its cubic symmetry under alloying alone, so

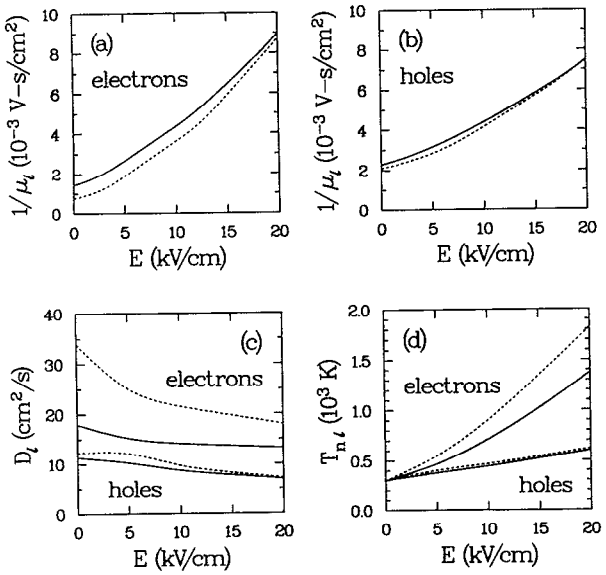

FIG. 5. Reciprocal differential mobility of (a) electrons and (b) holes, (c) longitudinal diffusion coefficient, and (d) longitudinal noise temperature for electrons and holes in unstrained silicon and bulk, unstrained $Si_{0.9}Ge_{0.1}$. In each figure, the solid lines pertain to $Si_{0.9}Ge_{0.1}$; the dotted lines pertain to silicon. In (c) and (d) the upper two curves are electron data and the lower two curves are hole data.

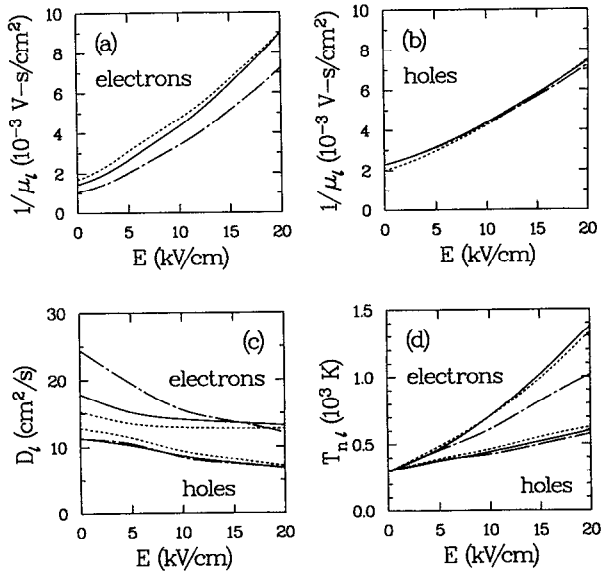

FIG. 6. Reciprocal differential mobility of (a) electrons and (b) holes, (c) longitudinal diffusion coefficient, and (d) longitudinal noise temperature for electrons and holes in unstrained $Si_{0.9}Ge_{0.1}$ and strained $Si_{0.9}Ge_{0.1}$/Si(001) ($\epsilon_{xx}=\epsilon_{yy}=-0.0042$, $\epsilon_{zz}=+0.0032$). In each figure the solid lines pertain to the unstrained alloy; the dotted lines pertain to the strained alloy with $E\|[100]$; the dotted-dashed lines pertain to strained alloy with $E\|[001]$. In (c) and (d) the upper three curves are electron data and the lower three curves are hole data.

⟨100⟩ still corresponds to six equivalent directions. However, random alloy scattering appears as an additional scattering mechanism, which acts to reduce the mobility and diffusion coefficient.

The effects of alloying alone on the reciprocal of the differential mobility μ_d, and the longitudinal diffusion coefficient D_l are shown in Figs. 5(a)–5(c). Here, data for the unstrained alloy $Si_{0.9}Ge_{0.1}$ are compared with those for unstrained silicon. For both electrons and holes the mobility and diffusion coefficient decrease with alloying, in the absence of strain. The noise temperature, being a function of D/μ, has a behavior with respect to alloying, that is dominated by the decrease in D. Thus, as shown in Fig. 5(d), the longitudinal noise temperature in unstrained $Si_{0.9}Ge_{0.1}$ is less than that in unstrained silicon.

The data of Fig. 5 indicate that, as a result of alloying, the longitudinal white noise spectral intensity S_l, which is proportional to D_l, is reduced by an amount that decreases with increasing electric field. Furthermore, the maximum longitudinal noise power, which is proportional to T_{nl}, also is reduced through alloying, but by an amount that increases with increasing electric field.

C. Effect of alloying and strain

The simultaneous effects of alloying and strain on the electron and hole transport properties are shown in Fig. 6. Qualitatively, the effect on mobility and diffusion is like that for strain alone (Fig. 3). However, since the strain is 0.42%, being less than half of the strain used in the strained silicon studies (Fig. 3), the magnitudes of the effects are correspondingly smaller in $Si_{0.9}Ge_{0.1}$/Si(001).

Therefore, the separation of the mobilities in the strained alloy from the mobilities in the unstrained alloy, shown in Figs. 6(a) and 6(b), generally follows the trends of the mobilities in strained and unstrained silicon, shown in Figs. 3(a) and 3(b) but to a smaller degree. A similar behavior is found for the diffusivities, shown in Fig. 6(c). The importance of the value of differential mobility in determining the noise temperature is again demonstrated for the strained alloy. In this case, the electron mobility for the strained alloy with the electric field in the plane of the film is not substantially different than the electron mobility for the unstrained alloy. Consequently, despite a resolvable difference in the respective diffusivities, the noise temperature for the two cases is very similar, as shown in Fig. 6(d). The electron noise temperature for the strained alloy, with the field perpendicular to the film, is substantially lower than the bulk material noise temperature, as in the case of silicon. This is again a consequence of the lower conductivity effective mass, leading to a higher carrier mobility.

The effect of alloying and strain on the thermal noise power spectral density is shown in Figs. 7(a) and 7(b), for electrons and holes, respectively. The electron and hole white noise bandwidths are only marginally larger for the strained alloy than for bulk silicon, both at thermodynamic equilibrium (zero field) and at $E=20$ kV/cm. Although some difference is found in the noise enhancement at high field and extremely high frequency (associated with the competing effects of momentum and energy relaxation[5]), from the standpoint of practical device considerations the thermal noise is white, and may be determined from the static diffusion coefficient.

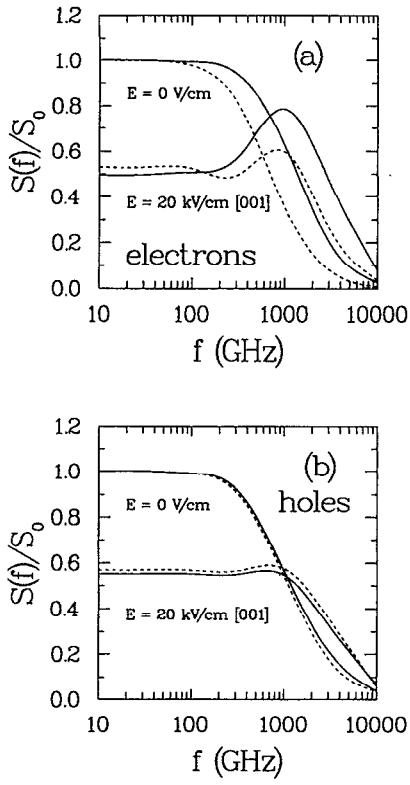

FIG. 7. Longitudinal noise spectral density for (a) electrons and (b) holes. The solid lines pertain to $Si_{0.9}Ge_{0.1}$/Si(001) and the dotted lines pertain to unstrained silicon. In each figure, the upper two curves are for $E \approx 0$ V/cm and the lower two curves are for $E = 20$ kV/cm, with $E \| [001]$. The data are normalized by the value of the longitudinal spectral density at zero field, zero frequency, S_0, in the respective materials.

IV. DISCUSSION

To summarize the results of this work, most of the diffusion and noise temperature characteristics are understandable in terms of the effect of strain and alloying on the conductivity effective mass involved in the transport. For electrons, the effect is qualitatively dependent on the orientation of the electric field, due to the large difference in the transverse and longitudinal effective masses in the ellipsoidal energy surfaces. For holes, the anisotropy with respect to field orientation is less pronounced. Generally, biaxial compressive strain reduces the hole effective mass, increasing the mobility and diffusivity; however, in the alloy the additional alloy scattering mechanism can offset the effect of reduced mass.

It was seen that intervalley scattering is significant for electrons in the bulk material with the effect of substantially increasing the overall diffusivity. With the field oriented perpendicular to the plane of the film, intervalley scattering is decreased under either positive or negative biaxial strain, which acts to separate the longitudinal and transverse valleys in energy. For in-plane strain on the order of 1%, intervalley diffusion is insignificant, causing a decrease to the diffusivity, potentially on the order of 30%. Since the noise spectral density S_l is proportional to the diffusivity, S_l will be reduced by the same amount under strain, for fields perpendicular to the film.

On the whole, the effect of alloying and strain on diffusion and noise characteristics is greatest at low fields and diminishes steadily as the field is increased. This is reasonable, since the effects of alloying and strain are greatest near the band edges. As carriers are heated by successively higher fields, they should be less affected by such band-structure changes.

ACKNOWLEDGMENTS

This work was supported by the U.S. Air Force (Grant No. AFOSR-91-0349) and by the U.S. Army URI program (DAAL03-92-G-0109).

[1] V. Sankaran, J. M. Hinckley, and J. Singh, IEEE Trans. Electron Devices **ED-40**, 1589 (1993), and references therein.
[2] T. P. Pearsall, CRC Crit. Rev. Solid State Mater. Sci. **15**, 551 (1989), and references therein.
[3] J. P. Nougier, *Physics of Nonlinear Transport in Semiconductors*, edited by D. K. Ferry, J. R. Barker, and C. Jacoboni (Plenum, New York, 1980), Vol. 52, p. 415.
[4] R. Fauquembergue, J. Zimmermann, A. Kaszynski, E. Constant, and G. Microondes, J. Appl. Phys. **51**, 1065 (1980).
[5] D. K. Ferry and J. R. Barker, J. Appl. Phys. **52**, 818 (1981).
[6] V. Bareikis, R. Barkauskas, A. Galdikas, and R. Katilyus, Sov. Phys. Semicond. **14**, 1046 (1980).
[7] C. Jacoboni, G. Gagliani, L. Reggiani, and O. Turci, Solid-State Electron. **21**, 315 (1978).
[8] C. Jacoboni and L. Reggiani, Rev. Mod. Phys. **55**, 645 (1983).
[9] L. Reggiani, *Physics of Nonlinear Transport in Semiconductors*, edited by D. K. Ferry, J. R. Barker, and C. Jacoboni (Plenum, New York, 1980), Vol. 52, p. 467.
[10] J. M. Hinckley and J. Singh, Phys. Rev. B **42**, 3546 (1990).
[11] J. H. Marsh, Appl. Phys. Lett. **41**, 732 (1982).
[12] J. M. Hinckley and J. Singh, J. Appl. Phys. **76**, 4192 (1994).
[13] J. M. Hinckley, Ph.D. thesis, University of Michigan, Ann Arbor, 1990.
[14] J. M. Hinckley and J. Singh, Phys. Rev. B **41**, 2912 (1990).
[15] S. H. Li, J. M. Hinckley, J. Singh, and P. K. Bhattacharya, Appl. Phys. Lett. **63**, 1393 (1993).
[16] S. M. Sze, *Physics of Semiconductor Devices*, 2nd ed. (Wiley, New York, 1981).
[17] B. K. Ridley, *Quantum Processes in Semiconductors* (Oxford University Press, Oxford, 1982).
[18] R. Brunetti, C. Jacoboni, F. Nava, L. Reggiani, G. Bosman, and R. J. J. Zijlstra, J. Appl. Phys. **52**, 6713 (1981).